Development of a high strength Al-Mg_2Si-Mg-Zn based alloy for high pressure die casting

Shouxun Ji*, Feng Yan, Zhongyun Fan
Brunel Centre for Advanced Solidification Technology (BCAST),
Brunel University London, Uxbridge UB8 3PH, United Kingdom
* Tel: +44-1895-266663, Fax: +44-1895-269758, Email: shouxun.ji@brunel.ac.uk

Abstract
A high strength Al-Mg_2Si-Mg-Zn based alloy has been developed for the application in high pressure die casting to provide improved mechanical properties. The effect of various alloying elements on the microstructure and mechanical properties including yield strength, ultimate tensile strength and elongation of the alloy was investigated under the as-cast and heat-treated conditions. The typical composition of the high strength alloy has been optimised to be Al-8.0wt.%Mg_2Si-6.0wt.%Mg-3.5wt.%Zn-0.6wt.%Mn (Al-11.0wt.%Mg-2.9wt.%Si-3.5wt.%Zn-0.6wt.%Mn) with unavoidable trace impurities. The mechanical properties of the alloy were enhanced by a quick solution treatment followed by ageing treatment. The improved tensile properties were at a level of yield strength over 300MPa, the ultimate tensile strength over 420MPa and the elongation over 3% assessed using international standard tensile samples made by high pressure die casting. The microstructure of the die-cast alloy consisted of the primary α-Al phase, Al-Mg_2Si eutectics, AlMgZn intermetallics and α-AlFeMnSi intermetallics under the as-cast condition. The AlMgZn intermetallic compound was dissolved into the Al-matrix during solution treatment and subsequently precipitated during ageing treatment for providing the effective improvement of the mechanical properties.
Key words: aluminium alloys; high pressure die casting; mechanical property; and microstructure.

1. Introduction

High pressure die casting (HPDC) is a well-developed manufacturing process and has been extensively used to cast aluminium alloys. In comparison with other casting methods, the advantages of HPDC process include [1,2]: (a) high productivity; (b) good dimensional accuracy and surface finish; (c) capable of providing high volume and economical production; (d) capable of making intricate shapes and thin wall castings; and (e) fine grain microstructure and good mechanical properties. However, the turbulent flow during die filling is an inherent problem in conventional HPDC process. This is fundamental for the formation of the internal defects [3,4], in particular porosities in die castings. Therefore it has limited the application of die castings as structural components [5, 6].

In the past two decades, the application of lightweighting materials in transportation has been the driving force to develop structural components using HPDC process [7]. The successful development of vacuum assisted HPDC has provided the capability of producing thin-wall castings with much reduced porosities [8]. Therefore, heat treatment is applicable to enhance the mechanical properties of die castings. However, the existing aluminium alloys for HPDC process are mainly based on Al-Si, Al-Si-Cu, and Al-Mg-Si systems [9,10]. Most of these alloys are not particularly suitable for the property enhancement by heat treatment, in particular not suitable for solution heat treatment. Although a quick solution treatment has been used for solution treatment of Al-Si-Cu alloys made by HPDC process [11], the currently available aluminium alloys is not satisfied with the increasing demands of manufacturing structural components by HPDC process. Therefore, the development of high strength aluminium alloys becomes significant to promote the application of aluminium alloys in transport and other fields where an improved strength and lightweight are essential.

The as-cast mechanical properties of the currently available aluminium alloys for HPDC process are listed in Table 1 [12,13], which shows that the hypoeutectic Al-Si based alloys provide yield strengths less than 200MPa with elongations over 3% and that the hypereutectic Al-Si based alloys provide yield strength at a level of 250MPa with elongations less than 1% under the as-cast condition. The recent study [11] has found that the heat treatment of cast Al-Si-Cu based alloys can significantly improve their strengths and the slight variation of alloy composition can significantly affect the mechanical properties of the alloy after heat treatment. However, studies of microstructure and mechanical properties of other commonly used aluminium alloying systems under as-cast and heat treatment conditions are limited. The present study attempts to investigate Al-Mg_2Si (Al-Mg-Si) system because of its attractive advantages [14,15], including the low cost of raw materials, low density of Mg_2Si and improved mechanical properties. Currently, due to the limitation of alloy composition, Al-Mg_2Si based alloys are normally cast using permanent mould or sand casting processes. The majority of the existing research on Al-Mg_2Si alloys are based on hyper-eutectic compositions [14,15]. The development of high strength aluminium alloys based on hypoeutectic Al-Mg_2Si system not only reduces the weight of existing aluminium castings by reducing the wall thickness, but also provides a heat treatable alloy with a lower solution temperature and shorter solutioning and ageing time.

In the present paper, we describe the effect of extra Mg, Mn and Zn in the Al-Mg_2Si system on the mechanical properties and microstructure of the cast alloys. The effect of solution and ageing heat treatment on the mechanical properties and microstructure was also studied. The composition was optimised for the alloy to provide yield strength over 300MPa, UTS over 420MPa and elongation over 3%. The discussion focuses on phase formation and microstructural characteristics with different alloying elements, and the correlation between microstructure and mechanical properties of the die-cast alloy.

2. Experimental

Pure aluminium, pure magnesium and pure zinc, Al-50wt.%Si and Al-20wt.%Mn master alloy ingots were used as the starting materials. Each of them was supplied at a specified composition with commercial purity. During experimental preparation, each element was weighed to a specified ratio with additional amounts for burning loss during melting. A melt of 10kg was prepared each time in a clay-graphite crucible using an electric resistance furnace. During melting, the temperature of the furnace was controlled to be 730±10°C. The ingots containing Al, Si and Mn elements were loaded into the crucible and melted first. Mg ingots and Zn ingots that had been preheated to 200°C were then carefully added into the completely melted alloy. After an hour of homogenisation, the melt was subjected to degassing, during which N_2 was input into the melt by a commercial rotatory degasser at 500rpm for 3 minutes and the top surface of the melt was covered by commercial granular flux during degassing. The melt was subsequently homogenised in the furnace for about 30 minutes before taking samples for composition measurement.

A mushroom casting with a bottom flat of ϕ60×10mm was made by a steel mould for composition analysis. The casting was cut off 3mm from the bottom and ground down to 800 grid SiC paper. The composition for onsite casting was obtained from an optical mass spectroscope (OMS), in which at least five spark analyses were tested and the average value was taken as the chemical composition of the alloy. After casting, some of the samples were further analysed by Inductively Coupled Plasma Mass Spectrometry (ICP-MS) and the results were taken as final composition of each alloy.

After OMS composition analysis and skimming, the melt was manually dosed and subsequently released into the shot sleeve of a 4500kN HPDC machine for making standard tensile samples. The pouring temperature was usually at 650^{o}C measured by a K-type thermocouple. A specially designed die was used to cast six ASTM standard samples with three ϕ6.35mm round samples and three flat samples for each shot (only round samples were used to assess the alloy's tensile property). The main dimensions of the die casting with overflow and biscuit are schematically shown in Figure 1. During casting, a water-based die releasing lubricant was used on the die block, which was pre-heated by the circulation of mineral oil at 250^{o}C in all shots. All casting samples were left on floor for at least 24 hours before testing their mechanical properties.

The round as-cast tensile samples were heat treated in an electric resistance furnace that was preheated to a given temperature and maintained the temperature consistently for at least one hour before putting the die-cast samples into the chamber of the furnace. The temperature inside the chamber was monitored by a separate thermocouple with a variation of ±2^{o}C during the heat treatment. The samples were water quenched immediately after solutioning treatment, but just taken out from the furnace for air cooling after ageing treatment.

The tensile tests were conducted following ASTM standard B557, using an Instron 5500 Universal Electromechanical Testing System equipped with Bluehill control software and a ±50kN load cell. All tensile tests were performed at an ambient temperature (~ 20^{o}C). The gauge length of the extensometer was 25mm and the ramp rate for extension was 2mm/min. Each set of data reported was based on the properties obtained from 10 to 20 samples.

The microstructure of each alloy was examined using a Zeiss optical microscope equipped with an AxioVision 4.3 Quantimet digital image analysis system for quantitative metallography, and a Zeiss SUPRA 35VP scanning electron microscope (SEM) equipped with energy dispersive spectroscopy (EDS). The metallographic samples were prepared by the standard technique. During optical microscope of the microstructure, five different fields of view were analysed for each specimen and the average was taken as the measured value. The quantitative SEM/EDS analysis was performed at an accelerating voltage of 20kV with calibration being carried out before each session. To minimise the influence from the interaction volume, five point analyses on selected particles or areas were conducted for each phase and the average was taken as the measurement. Transmission electron microscope (TEM) analysis was performed using a JEOL-2100F microscope. The specimens for the TEM analysis were prepared by electrolytic polishing with a solution of nitric acid and methyl alcohol (2:8 in volume) at a voltage of 22V and a temperature between -20°C and -30°C.

3. Results

Mg_2Si is a compound composed of Mg and Si elements, where the compound forms at the atom ratio of Mg:Si=2:1, and the weight ratio of Mg:Si = 1.73:1. The Mg_2Si crystal occurs during solidification because the maximum solid solubility of Si into Mg is less than 0.03% [16]. Al-Mg_2Si can be recognised as a simple pseudo-binary alloy. This is particularly useful to simplify the thermodynamics of Al-Mg-Si system with a specific ratio in a binary phase diagram. However, the experiments were carried out using individual element and it is easier to understand using Mg and Si. To balance the need in thermodynamics calculation and experimental confirmation, the corresponding compositions of Mg_2Si, Mg and Si are listed in Table 2.

3.1 Effect of extra Mg in Al-Mg_2Si alloys

Figure 2 shows the equilibrium phase diagrams at Al-rich side for Al-Mg_2Si system and the Al-Mg_2Si-Mg ternary system on the cross section of 8wt.%Mg_2Si (5.07wt.%Mg-2.93wt.%Si), respectively. The pseudo-binary Al-Mg_2Si system (Figure 2a) behaves like a normal binary eutectic system with a eutectic point at 13.9 wt.% Mg_2Si (Al-8.81wt.%Mg-5.09wt.%Si). It is seen that a narrow three-phase region for L+α-Al+Mg_2Si co-existence between 591 °C and 578 °C. With extra Mg in the Al-Mg_2Si system, the shape of equilibrium phase diagram exhibits little change. However, the eutectic point is shifted towards a lower Mg_2Si concentration and the area of co-existence for the three phases is enlarged. This means that, for a given Mg_2Si content, an extra Mg addition results in a decrease of the volume fraction of the primary α-Al phase and an increase of the volume fraction of Al-Mg_2Si eutectic phase. To confirm this observation, calculations were performed for different extra Mg contents and the calculated results are summarised in Table 3. It is seen that the solidification parameters are altered by the extra Mg in the Al-Mg_2Si system. The eutectic points are significantly shifted to the Al-rich side and the solidification range is increased with increasing extra Mg. Figure 2b shows the equilibrium phase diagram of Al-Mg_2Si-Mg ternary system on the cross section of 8wt.%Mg_2Si (5.07wt.%Mg-2.93wt.%Si). It is seen that β-AlMg phase is formed when extra Mg is more than 2 wt.%. Meanwhile, the primary phase can be varied with extra Mg content, indicating that extra Mg can be used to introduce different phases in the Al-Mg_2Si based alloys.

To confirm the calculated results, a series of experiments were performed with different amounts of extra Mg in the Al-Mg_2Si alloys. The representative microstructures are shown in Figure 3 and the volume fractions of different phases are shown in Figure 4. The primary phase presented in the as-cast microstructure was different. With 1.9wt.% extra Mg in Figure 3a and 4a, the alloy showed a typical hypoeutectic microstructure, consisting of dendrites or fragmented dendrites of primary α-Al phase surrounded by Al-Mg_2Si eutectic phase. Similarly, when the extra Mg was at 4.1 wt.% in Figure 3b and 4a, the alloy also presented a typical hypoeutectic microstructure. However, the primary α-Al phase exhibited a much lower volume fraction and the Al-Mg_2Si eutectic showed a much higher volume fraction in comparison with that shown in Figure 3a. Moreover, the microstructure was much different when the extra Mg was 5.8 wt.% (Figure 3c and 4a). The coarse primary α-Al phase almost disappeared and the microstructure was dominated by fine primary α-Al phase and Al-Mg_2Si eutectics. When the extra Mg was increased further to 7.6 wt.% (Figure 3d and 4a), the primary phase was the polygonal Mg_2Si phase. The Mg_2Si particles had an average size of 20 μm and were randomly distributed in the matrix. The changes in the Al-9.9 wt.%Mg_2Si (Al-6.27wt.%Mg-3.63wt.%Si) and Al-12.7

wt.%Mg_2Si (Al-8.05wt.%Mg-4.65wt.%Si) systems showed a similar trend but with different eutectic reaction points at different extra Mg contents, where the volume fraction of primary phase was close to zero as shown in Figure 4. Because the Al-Mg_2Si alloys without extra Mg had a severe die soldering problem, the microstructure of die-cast Al-Mg_2Si alloys was unable to be presented. However, the experimental results shown in Figures 3 and 4 were generally consistent with the calculation results shown in Figure 2 and Table 3.

In addition to the primary phase, it was found that the eutectic Al-Mg_2Si phase formed during HPDC was different in the experimental alloys. Figure 5 shows the microstructure of the as-cast Al-7.8wt.%Mg_2Si-5.8wt.%Mg (Al-10.75wt.%Mg-2.86wt.%Si) alloy. In Figure 5a, the coarse Mg_2Si phase with a larger eutectic spacing was found in the matrix, in which some of the eutectics were divorced. In Figure 5b, only regular eutectic were found in the matrix. Meanwhile, AlMg intermetallics were also observed in the microstructure. This is consistent with the thermodynamical calculation shown in Figure 2.

Figure 6 shows the yield strength, UTS and elongation of the as-cast Al-Mg_2Si-Mg alloys. In general, the yield strength was increased with increasing Mg content, but showed no significant difference with increasing Mg_2Si phase (Figure 6a). Conversely, the elongation was decreased with the increase of Mg and Mg_2Si in the alloys (Figure 6c). The UTS were different for the alloys with different extra Mg content (Figure 6b). The decrease of the UTS was significant for the Al-9.9wt.%Mg_2Si (Al-6.27wt.%Mg-3.63wt.%Si) and Al-12.7wt.%Mg_2Si (Al-8.05wt.%Mg-4.65wt.%Si) alloys with the increase of extra Mg in the alloys. However, for the Al-7.8wt.%Mg_2Si (Al-4.95wt.%Mg-2.86wt.%Si) alloy, the UTS was increased when the extra Mg was below 5.8 wt.%, and was decreased for the further increase of the extra Mg over 5.8 wt.%. The Al-7.8wt.%Mg_2Si (Al-4.95wt.%Mg-2.86wt.%Si) alloy with 5.8 wt.% extra Mg provided a yield strength of 170 MPa, an elongation of 6.9% and a UTS of 340 MPa, which is an optimised combination of strengths and ductility. However, it is noted that the yield strength is much lower than the target of 300MPa. Therefore, further improvement is conducted as described in the following sections.

3.2 Effect of Mn in Al-Mg_2Si-Mg alloys

Figure 7 shows the tensile properties of the Al-7.8wt.%Mg_2Si-5.8wt.%Mg (Al-10.75wt.%Mg-2.86wt.%Si) alloy with different amounts of Mn addition under as-cast condition. The increase of Mn content in the alloys resulted in a slight increase of the yield strength and UTS, but a slight decrease of the elongation. The elongation was decreased from 6.9% to 6.5% when the Mn content was increased from 0.19wt.% to 0.59wt.%, which is the level of the commonly used in the die-cast Al-Mg-Si alloy.

Figure 8 shows the typical microstructure of the intermetallics in the Al-7.8wt.%Mg_2Si-5.8wt.%Mg-0.59wt.%Mn (Al-10.75wt.%Mg-2.86wt.%Si-0.59wt.%Mn) alloy containing 0.12 wt.% Fe. Intermetallics with two different sizes were observed and the volume fraction of the intermetallics increased with the increase of Mn addition. The quantitative analysis showed that the average size of the fine intermetallics were about 0.8μm. The volume fraction of the Mn-rich intermetallics was shown in Figure 9 for the Al-Mg_2Si-Mg alloys with various Mn levels. An obvious increase of the volume fraction could be seen for the increasing Mn content. The composition of the Mn-rich intermetallic phase was measured with different amounts of Mn additions and the results are shown in Table 3. Clearly, the Mn-rich intermetallics were α-AlFeMnSi phase according to the morphology and composition. The measured constituent of the intermetallics could be described by $Al_{42-46}(Fe,Mn)_{3.5-7}Si$.The Mn-rich intermetallics are essentially associated with Fe in the die cast alloys, although it is different to the frequently observed $Al_{15}(Fe,Mn)_3Si_2$ intermetallics in aluminium alloys [17].

3.3 Effect of Zn in Al-Mg_2Si-Mg-Mn alloys

Different amounts of Zn were added into the Al-7.8wt.%Mg_2Si-5.8wt.%Mg-0.59wt.%Mn (Al-10.75wt.%Mg-2.86wt.%Si-0.59wt.%Mn) alloy. Figure 10 shows the effect of Zn on the tensile properties of Al-7.8wt.%Mg_2Si-5.8wt.%Mg-0.59wt.%Mn (Al-10.75wt.%Mg-2.86wt.%Si-0.59wt.%Mn) alloy under as-cast condition. The increase of Zn content in the alloys resulted in a significant increase of the yield strength and a significant decrease of the elongation while the UTS were maintained. When Zn content was 3.51wt.%, the elongation was still higher than 2% and the yield strength was at a level of 250MPa and the UTS was at a level of 350MPa.

The typical microstructure of the experimental alloy is shown in Figure 11. An AlMgZn phase was observed, which were characterised by irregular shapes, as shown in Figure 12. The Zn-containing intermetallic compounds were located at the boundaries of the primary α-Al phase or between the eutectic cells and the primary α-Al phase. The measured volume fractions of the AlMgZn phase are shown in Figure 13, which was increased significantly with the increasing Zn addition. The constituent of the AlMgZn phase was analysed by SEM/EDS and the results are shown in Table 4. The quantitative measurement confirmed that the intermetallic compounds contained 25±1 at.% Mg, 10±0.7 at.% Zn, which corresponded to a formula of $Al_{13}Mg_5Zn_2$. Therefore, the Zn-rich intermetallic phase was essentially the same compound in the experimental alloys.

3.4 Effect of solution and ageing in Al-Mg_2Si-Mg-Zn-Mn alloys

Solution and ageing treatments were performed at 490°C and 180°C, respectively [18]. Figure 14 shows the effect of Zn on the yield strength, UTS and elongation of the alloys after solution and ageing heat treatment. Significant increases in yield strength and UTS and a decrease in elongation were observed in the alloy with increasing the Zn content. Although the results in Figures 10 and 14 showed a similar trend, the tensile properties of the alloy after solution and ageing were significantly higher than that under as-cast condition. The tensile properties can be easily achieved at a level of 340MPa of yield strength, 430MPa of UTS and 3.5% of elongation.

The typical microstructures after solution at 490°C are shown in Figure 15. It is seen that the AlMgZn intermetallics were gradually dissolved into the matrix at 490°C. After 15 minutes, the AlMgZn phase almost disappeared, indicating its completed dissolution into the matrix. However, no obvious change was observed for the AlFeMnSi intermetallics and eutectic Mg_2Si phase after the solution treatment. The TEM micrograph shown in Figure 16 revealed that a large numbers of fine MgZn precipitates were formed in the α-Al phase after solutioning and ageing. This confirmed that AlMgZn irregular intermetallic phase was dissolved into the matrix during solution treatment and then precipitated in the form of fine particles during ageing to provide strengthening to the alloy. The typical as-cast microstructure of the optimised Al-7.8wt.%Mg_2Si-4.8wt.%Mg-3.5wt.%Zn-0.59wt.%Mn (Al-10.75wt.%Mg-2.86wt.%Si-0.59wt.% Mn -3.51wt.%Zn) alloy shown in Figure 14a consisted of α-Al primary phase, eutectic Al-Mg_2Si phase, β-AlMgZn phase, and α-AlFeMnSi phase. The volume fraction of the primary α-Al phase was typically at a level of less than 15%. The Al-Mg_2Si eutectics showed a combination of divorced eutectics and conventional

lamellar eutectics. The lamellar eutectics exhibited a relatively high volume fraction and were usually located between the primary particles. The β-AlMgZn phase was the dominant intermetallics in the as-cast state. The amounts of α-AlFeMnSi particles were at very low level in the alloy. The β-AlMgZn phase in the same alloy showed a significant change after heat treatment. The irregular β-AlMgZn phase was decomposed during solution treatment and was precipitated as fine particles in the primary α-Al phase during ageing.

4. Discussion

4.1 Effect of alloying elements on the microstructural formation during HPDC

In the experimental alloys, different elements were added aiming to provide strengthening through both solution strengthening and secondary phase strengthening via the formation of different phases during HPDC and the subsequent heat treatment. In the Al-Mg_2Si system with extra Mg, the formation of Al-Mg_2Si eutectic phase is enhanced during solidification, although the primary α-Al phase is still prior phase due to the hypoeutectic composition. As the maximum solid solubility of Mg in Al is 17.4wt.% and Mg_2Si in Al is 1.85wt.% under equilibrium condition [16], the solution strengthening can make a major contribution to the mechanical properties. Meanwhile, the Mg_2Si content is over the maximum solubility, leading to the formation of Al-Mg_2Si eutectic phase. The Mg_2Si phase can pin the dislocations and grain boundaries to slow their sliding under stress. Therefore, the combination between Mg_2Si and extra Mg content increases the strengths with an appropriate ductility in the aluminium alloys.

The addition of Mn forms an intermetallic phase in Al-Mg_2Si-Mg alloys because of its low solubility in Al [19]. Because Fe is always associated in die-cast alloys, the Mn-rich intermetallics are actually the (Fe,Mn)-rich intermetallic phase. Although several types of intermetallic phases can be formed in cast aluminium alloys, the hexagonal shaped α-AlFeMnSi is the common one when Mn is added at a level of $Mn/Fe \geq 0.5$ [20, 21]. Several formats have been reported for the α-AlFeMnSi compounds, including $Al_{16}(Fe,Mn)Si_3$ [22] and $Al_{15}(Fe,Mn)_3Si_2$ [23]. Fang *et al.* [24] suggested that the stoichiometry of the quaternary α-AlFeMnSi phase for Al-Si based alloys is best described by $Al_{15}(Fe,Mn)_3Si_2$. In the present study, according to the equilibrium phase diagram of the Al-Mg_2Si-Mg-Mn alloy (Figure 17), the prior phase is changed to α-AlFeMnSi when Mn concentration is higher than 0.37wt.%. SEM/EDS analysis confirms that the intermetallics is α-AlFeMnSi with a stoichiometry of $Al_{13\text{-}21}(Fe,Mn)_{1\text{-}3}Si_{0.25\text{-}0.5}$. In comparison with the best described α-AlFeMnSi phase, the intermetallics found in the present study contain less Si. This can possibly be attributed to the less Si in the experimental alloys. During solidification, the formed α-AlFeMnSi prior phase has a very low volume fraction and is pushed to the front of solidification interface. Consequently, the Fe- and Mn-rich intermetallics are settled in the interdendritic regions.

Zinc improves the mechanical performance of the Al alloys under heat treatment condition by providing both solution strengthening and precipitation strengthening via the formation of intermetallics [10]. The maximum solubility of Zn in Al is 67 at.% at 381^{o}C, which is the largest one among all the elements [25]. Therefore Zn and Al are usually not to form intermetallic phases at elevated temperatures. However, the maximum solubility of Zn in Al is 0.85 at.% at 25^{o}C, therefore Zn-rich intermetallic phase will form in the as-cast microstructure. The addition of Zn to the Al-Mg alloy system reduces the solid solubility of Mg in Al, promoting the formation of AlMgZn intermetallic phase during solidification. The majority of AlMgZn intermetallics are distributed along the grain boundaries with irregular shapes. Meanwhile, the increasing Zn content increases the amount of intermetallics in the microstructure and can be presented as a continuous network at grain boundaries. Therefore, the strength enhancement from the intermetallics is a balance of different factors. On the other hand, AlMgZn intermetallics can be decomposed and dissolved into the aluminium matrix during solutioning treatment at a relatively low temperature in comparison with AlCu and AlMgSi compounds and subsequently precipitated during ageing. This will improve the strength of the alloy. Therefore, the addition of Zn needs to be carefully controlled in order to have a good balance for property improvement.

4.2 Microstructural characteristics of the Al-Mg_2Si-Mg-Zn alloy

In the Al-Mg_2Si-Mg-Zn alloy, the as-cast microstructure contains several phases formed during solidification, including primary α-Al, eutectic Al-Mg_2Si, β-AlMgZn and α-AlFeMnSi phases. The microstructural characteristics of the alloy can be understood from the solidification and phase formation process. Figure 18 shows the equilibrium phase diagram of the Al-Mg_2Si-Mg-Zn-Mn system on the cross section of Al- 8 wt.% Mg_2Si - 6 wt.% Mg - 0.6 wt.% Mn calculated by Pandat software. It is seen that the solidification sequence of the alloy is L→ α-Al + Mg_2Si +AlMgZn + AlFeMnSi + AlMg when Zn is within the calculation range. The prior phase is α-AlFeMnSi, followed by the formation of other phases with temperatures being reduced. However, the calculation results are slightly different to the experimental results where no AlMg phase was actually found in the experimental results. The disappearance of the AlMg intermetallics is mainly because of the existence of Zn in the alloy. Although the exact mechanism is still not clear, the formation temperatures of both AlMg and AlMgZn intermetallics is close to each other according to the equilibrium shown in Figures 2 and 18. Given non-equilibrium solidification, the AlMgZn phase is formed before AlMg phase, resulting in suppression of the AlMg phase.

4.3 Microstructure-properties relationship

As mentioned earlier, the microstructure in the die castings compromises the primary α-Al phase, Al-Mg_2Si eutectics and intermetallic phases. Mg, Si, Zn and Mn can provide solution strengthening to the α-Al phase. The precipitates of intermetallics under as-cast condition can strengthen the alloy by acting as pins to prevent dislocations from sliding under stress. Therefore, the fine and compact α-AlFeMnSi phase can reduce the detrimental effect of needle-shaped intermetallics. However, the intermetallics themselves are brittle and can initialise cracks, resulting in the reduction in ductility. The further strengthening by solution and ageing heat treatment results from the precipitation of MgZn phase in the α-Al phase. The AlMgZn compounds decompose during solution and subsequently precipitate during ageing. The fine precipitates provide much more effective strengthening effect in the alloy, during which the detrimental effect from irregular AlMgZn phase is minimised and the elongation is thus improved. On the other hand, during heat treatment, no significant change is observed for the α-AlFeMnSi and Mg_2Si phase because of their high thermal stability, indicating that the enhancement in mechanical properties from the α-AlFeMnSi and Mg_2Si intermetallics is limited after the heat treatment.

5. Conclusions

(1) A high strength aluminium alloy for high pressure die casting has been developed based on Al-Mg_2Si-Mg-Zn system. The typical tensile properties of the die-cast alloy are 300MPa of yield strength, 420MPa of ultimate tensile strength, and 3% of elongation under solution and aged condition.
(2) The typical composition of the high strength aluminium alloy comprises of 8.0wt.%Mg_2Si, 6.0wt.%Mg, 3.5wt.%Zn, 0.6wt.%Mn (Al-11.0wt.%Mg-2.9wt.%Si-3.5wt.%Zn-0.6wt.%Mn), with the unavoidable impurity elements.
(3) The die-cast high strength Al-Mg_2Si-Mg-Zn alloys consists of primary α-Al, Al-Mg_2Si eutectics, β-AlMgZn, and α-AlFeMnSi phases in the as-cast microstructure. The solution treatment decomposes the AlMgZn intermetallics into Al matrix and fine Zn-rich intermetallics are precipitated during the subsequent ageing treatment. Heat treatment significantly improves the tensile properties of the Al-Mg_2Si-Mg-Zn based alloy.
(4) Zinc is an applicable alloying element in the Al-Mg_2Si-Mg alloys to increase the tensile strength under both as-cast and heat treated conditions with a scarification of the ductility. Appropriate level of Zn content is essential to achieve such a high level of mechanical properties for the Al-Mg_2Si-Mg-Zn based alloys.

Acknowledgements
The financial support is gratefully acknowledged for the Engineering and Physical Sciences Research Council (EPSRC), Technology Strategy Board (TSB) and Jaguar Land Rover (JLR), United Kingdom.

Table 1 Typical mechanical property of currently registered aluminium alloys for HPDC process.

Alloy	Alloy System	Temper	UTS (MPa)	Yield Strength (MPa)	Elongation (%)
360	Al-Si-Mg	As-cast	305	170	3
A360.0	Al-Si-Mg	As-cast	315	165	4
380	Al-Si-Cu	As-cast	315	160	3
A380.0	Al-Si-Cu	As-cast	325	160	4
383	Al-Si-Cu	As-cast	310	150	4
384	Al-Si-Cu	As-cast	330	165	3
390	Al-Si-Cu-Mg	As-cast	280	240	<1
B390.0	Al-Si-Cu-Mg	As-cast	315	250	<1
392	Al-Si-Cu-Mg	As-cast	290	270	<1
413	Al-Si	As-cast	295	145	3
A413.0	Al-Si	As-cast	290	130	4
C443.0	Al-Si	As-cast	230	95	9
518	Al-Mg	As-cast	310	193	5

Table 2 The relationships among Mg_2Si, Mg and Si in Al-Mg_2Si system.

Mg_2Si (wt.%)	Mg (wt.%)	Si (wt.%)
6	3.80	2.20
8	5.07	2.93
10	6.34	3.66
12	7.61	4.39
13	8.24	4.76

Table 3 Calculated results for the effect of extra Mg on the eutectic reaction of Al-Mg_2Si alloys.

Extra Mg (wt.%)	0	4	6	8	10
Al-Mg_2Si eutectic reaction point (wt.%)	13.9	9.7	8.1	6.4	5.1
Starting temperature for eutectic reaction (°C)	591	590	590	586	582
Finishing temperature for eutectic reaction (°C)	578	563	556	531	505
Transit zone of eutectic reaction (°C)	13	27	34	55	77

Table 4 Composition of the Mn-rich intermetallic phase in the Al-7.8 wt.%Mg_2Si-5.8 wt.%Mg-xMn-0.12wt.%Fe (Al-10.75wt.%Mg-2.86wt.%Si-xMn-0.12wt.%Fe) alloys measured by quantitative SEM/EDS analysis

Mn concentration	Identified composition	Al	Fe	Mn	Si
0.19	$Al_{45.5}(Fe,Mn)_{3.5}Si$	91.72	4.28	2.12	1.87
0.41	$Al_{45.5}(Fe,Mn)_{3.5}Si$	91.25	4.51	2.13	2.11
0.59	$Al_{42}(Fe,Mn)_{7}Si$	85.41	6.24	6.41	1.93
0.78	$Al_{42}(Fe,Mn)_{7}Si$	84.23	6.92	6.82	2.03

Table 4 Composition of Zn-rich intermetallic phase in the Al-7.8 wt.% Mg_2Si - 5.8 wt.% Mg -0.58 wt.% Mn-xZn (Al-10.75wt.%Mg-2.86wt.%Si-0.58wt.%Mn-xZn) alloys measured by the quantitative SEM/EDS analysis.

Zn (wt.%)	Identified composition	Al	Mg at%	Zn
0.97	$Al_{13}Mg_5Zn_2$	66.15	24.01	9.84
1.87	$Al_{13}Mg_5Zn_2$	65.23	25.25	9.52
2.56	$Al_{13}Mg_5Zn_2$	65.18	24.38	10.45
3.51	$Al_{13}Mg_5Zn_2$	64.59	24.85	10.56

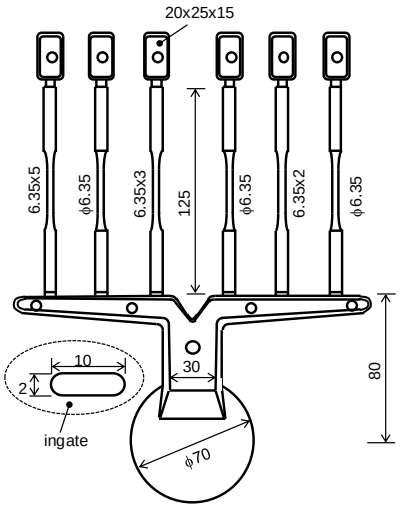

Figure 1 Diagram of die casting for the standard tensile testing samples of cast aluminium alloy according to the specification defined in ASTM B557-06. The overflow and biscuit are designed in association with the cold chamber die casting machine. The dimensions are in mm.

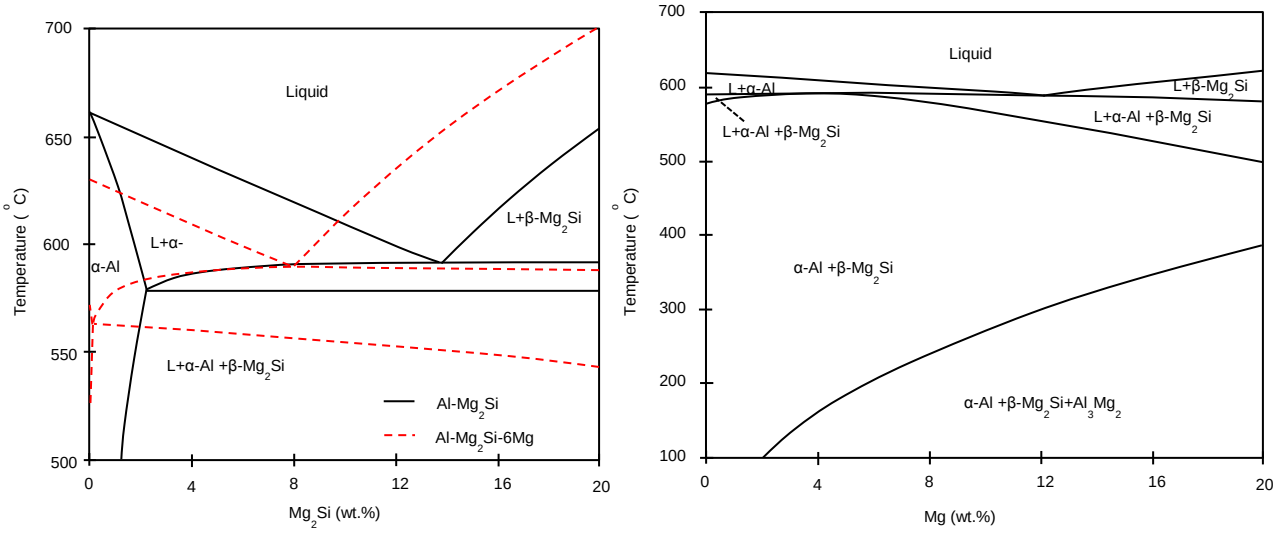

Figure 2 Equilibrium phase diagrams calculated by Pandat software (a) Al-Mg_2Si pseudo-binary system and Al-Mg_2Si-Mg ternary system with 6wt.%Mg, and (b) Al-Mg_2Si-Mg ternary system on the cross section of Al-8wt.%Mg_2Si (Al-5.07wt.%Mg-2.93wt.%Si).

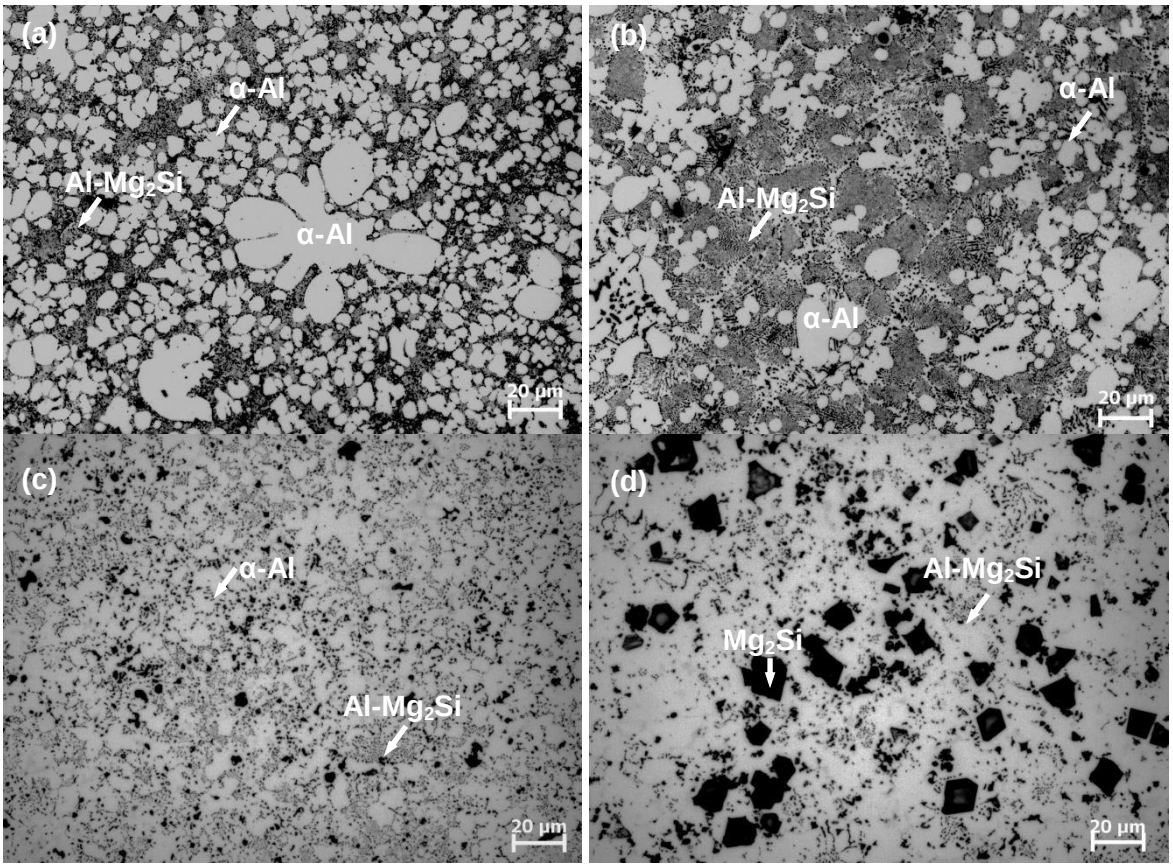

Figure 3 Optical micrographs showing the effect of excess Mg on the as-cast microstructure of Al-7.8 wt.%Mg_2Si (Al-4.95wt.%Mg-2.86wt.%Si) alloy with (a) 1.9wt.%Mg, (b) 4.1wt.%Mg, (c) 5.8wt.%Mg, and (d) 7.6wt.% Mg.

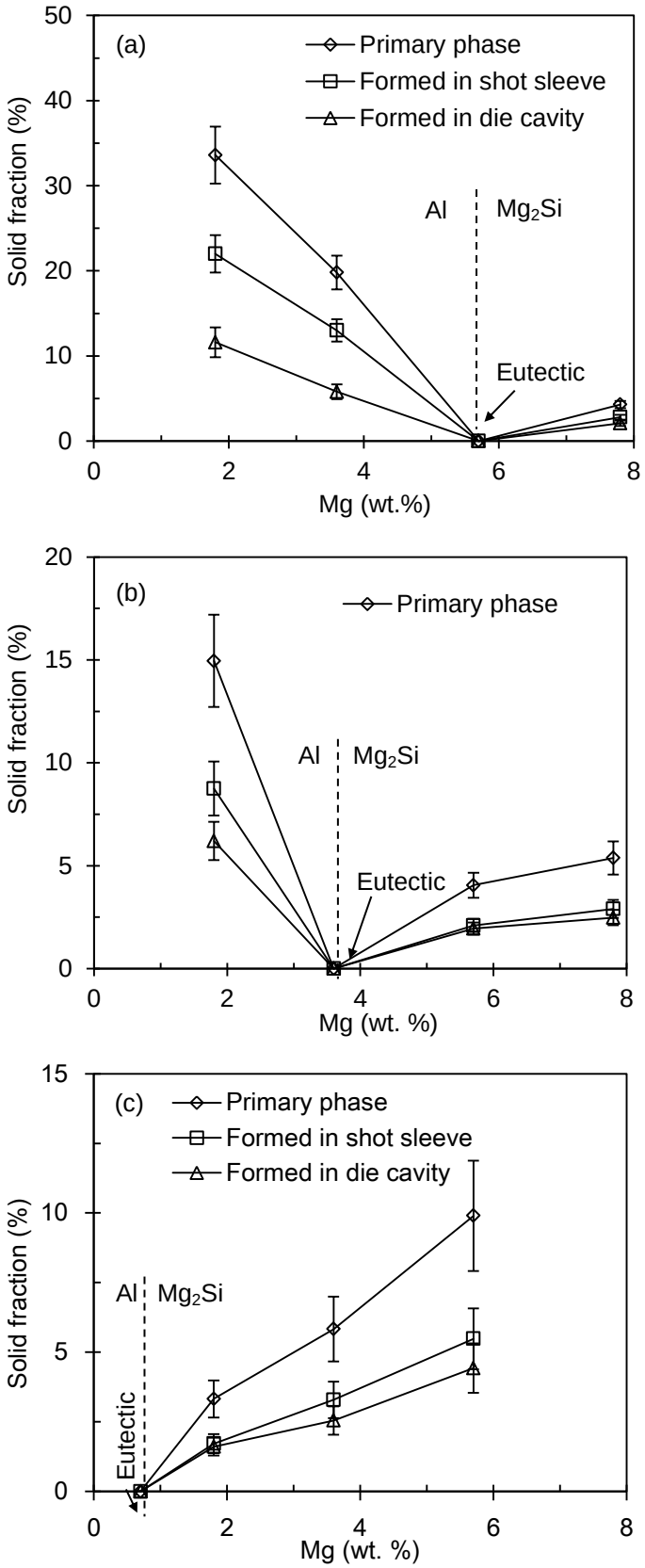

Figure 4 The solid fraction of primary phases in the Al-Mg_2Si-Mg alloys with different levels of extra Mg in (a) Al-7.8 wt.%Mg_2Si (Al-4.95wt.%Mg-2.86wt.%Si), (b) Al-9.9 wt.%Mg_2Si (Al-6.27wt.%Mg-3.63wt.%Si), and (c) Al-12.7 wt.%Mg_2Si (Al-8.05wt.%Mg-4.65wt.%Si) alloys.

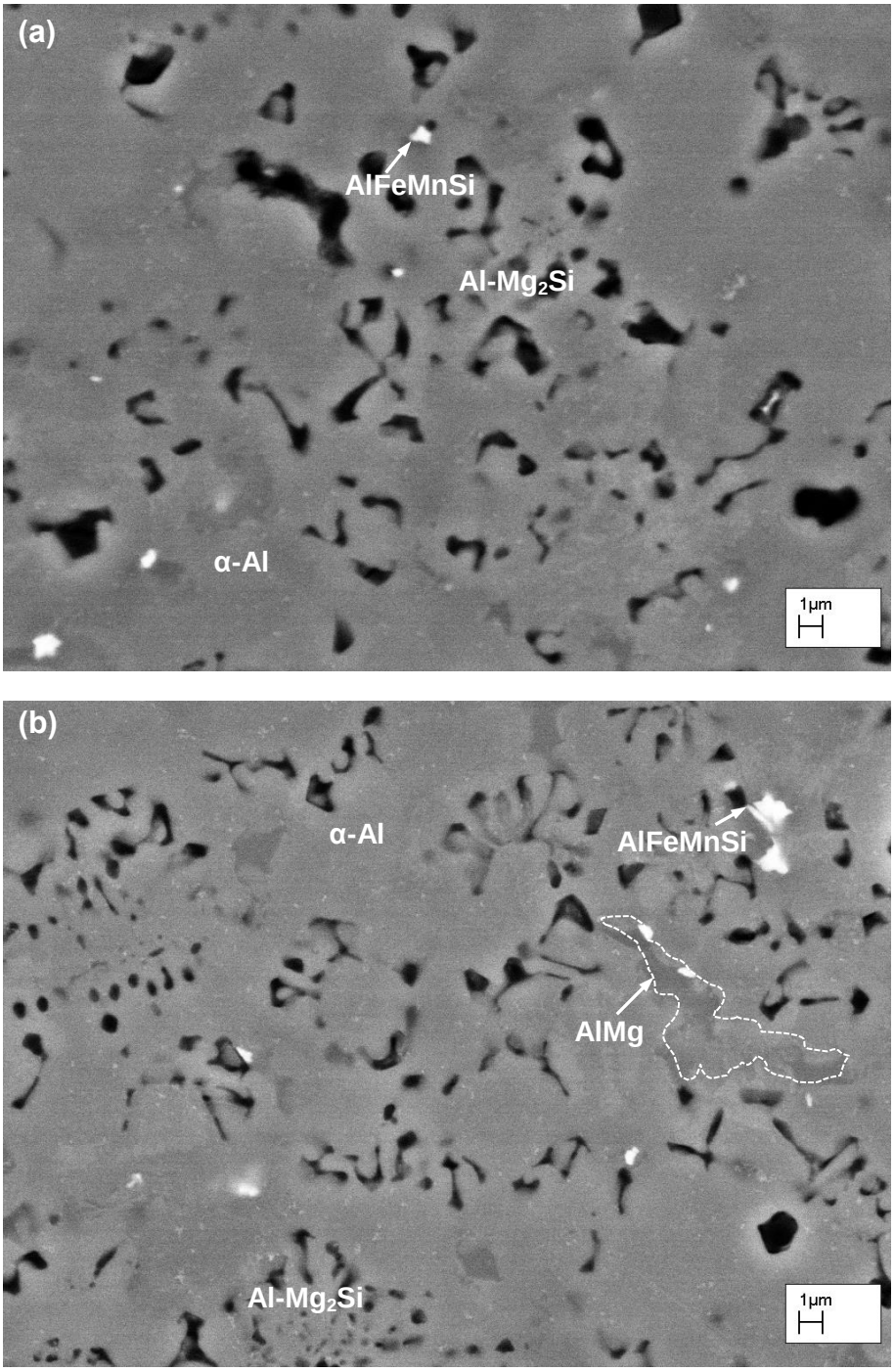

Figure 5 Backscattered SEM images showing the eutectic microstructure of the Al-7.8 wt.%Mg_2Si-5.8 wt.%Mg (Al-10.75wt.%Mg-2.86wt.%Si) alloy, (a) the eutectics formed in the shot sleeve and (b) the eutectics formed in the die cavity.

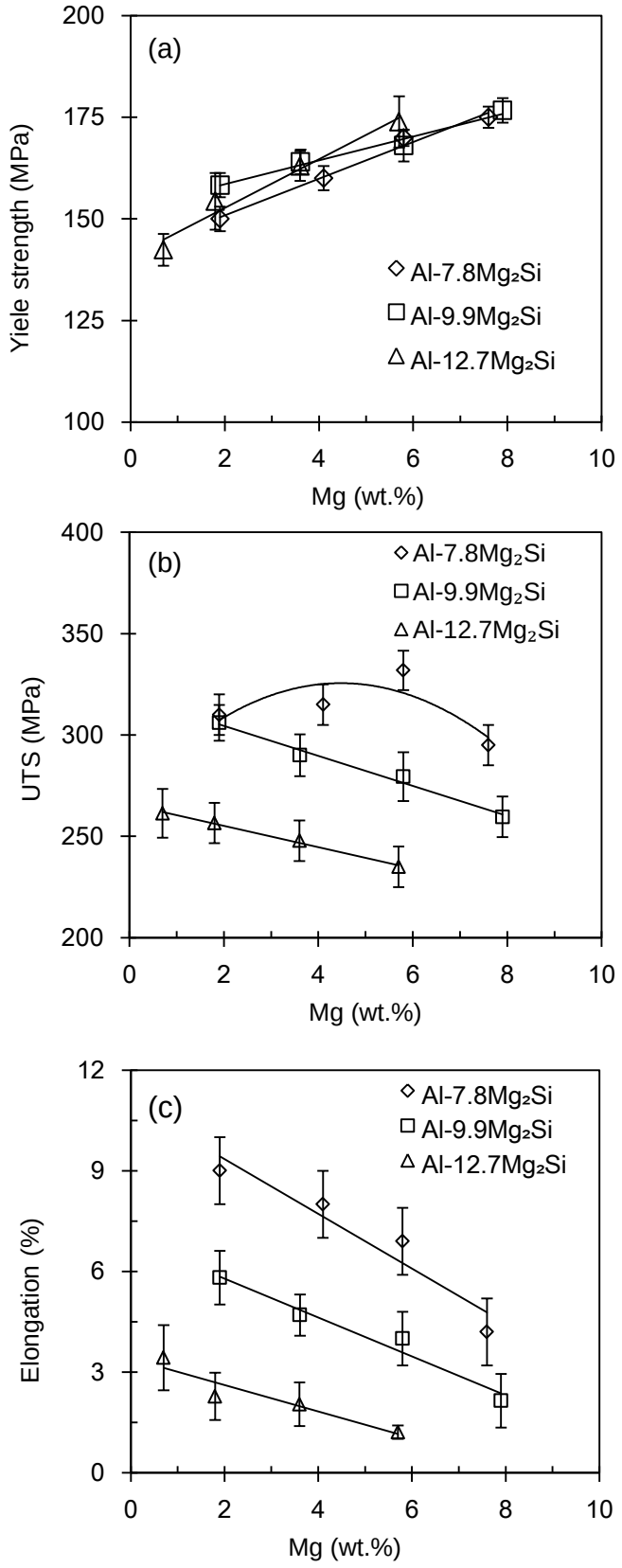

Figure 6 Effect of extra Mg on the mechanical properties of Al-Mg_2Si alloys under as-cast condition, (a) yield strength, (b) ultimate strength (UTS), and (c) elongation.

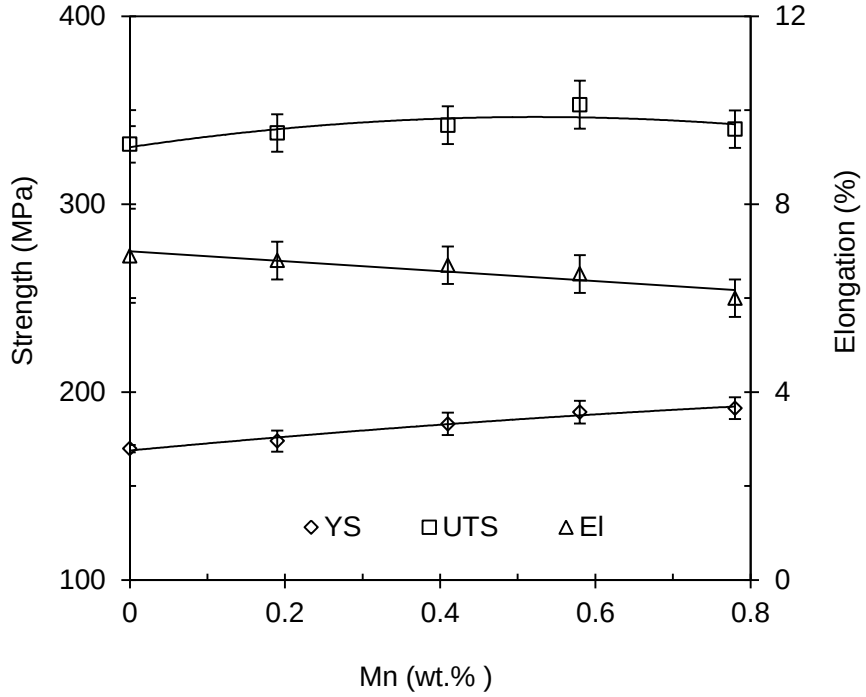

Figure 7 Effect of Mn content on the yield strength (YS), ultimate tensile strength (UTS) and elongation (El) of the Al-7.8wt.%Mg_2Si-5.8wt.%Mg-xMn-0.12wt.% Fe (Al-10.75wt.%Mg-2.86wt.%Si-xMn-0.12wt.%Fe) alloys under as-cast condition.

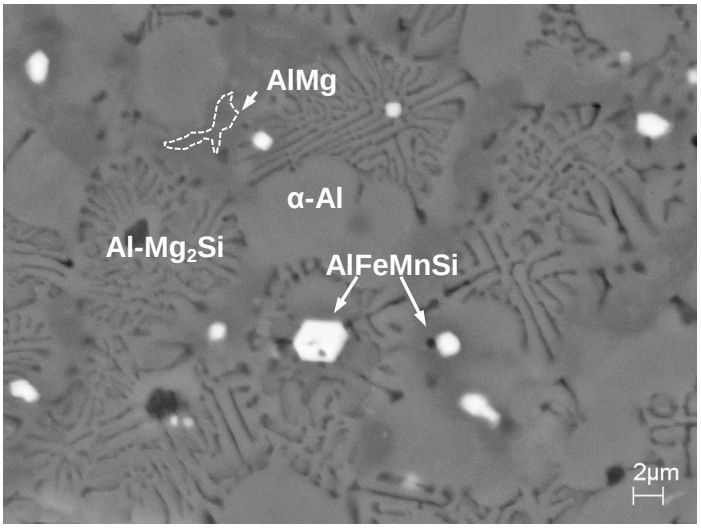

Figure 8 Backscattered SEM micrograph showing the morphology of Mn-rich intermetallic phase and AlMg intermetallic phase in the Al-7.8 wt.%Mg_2Si-5.8 wt.%Mg-0.59wt.%Mn (Al-10.75wt.%Mg-2.86wt.%Si-0.59wt.%Mn) alloy with 0.12wt.%Fe.

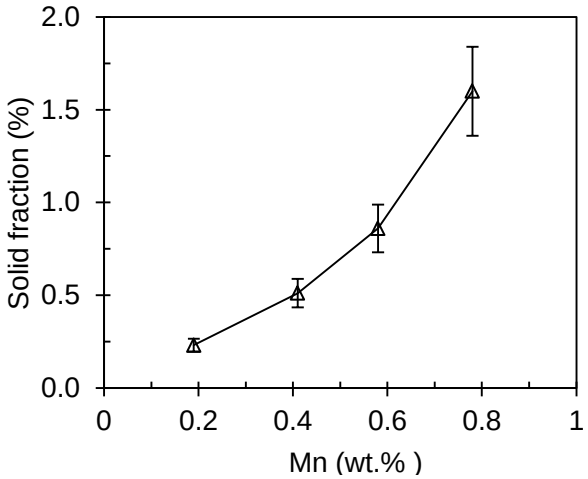

Figure 9 Effect of Mn content on the solid fraction of Mn-rich intermetallic phase in the Al-7.8 wt.%Mg_2Si-5.8 wt.%Mg-xMn (Al-10.75wt.%Mg-2.86wt.%Si-xMn) alloys with 0.12wt.%Fe.

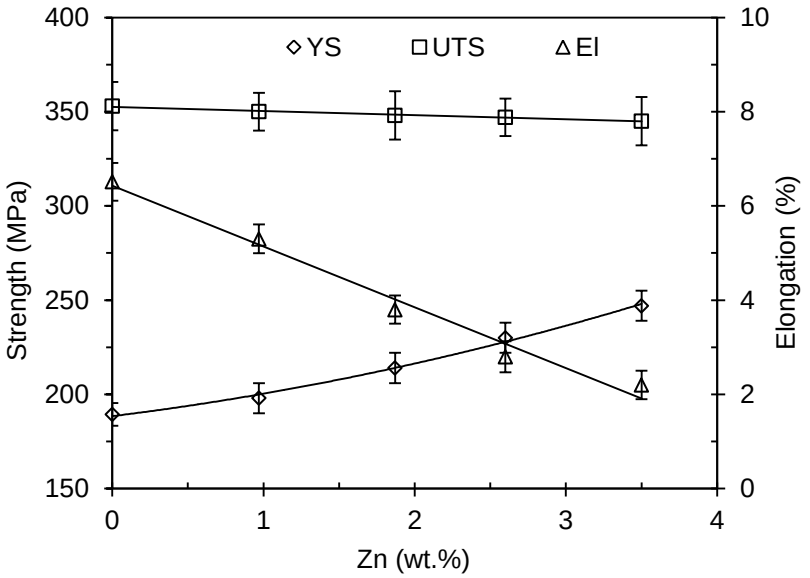

Figure 10 Mechanical properties of the Al-7.8wt.%Mg_2Si-5.8 wt.%Mg-0.59wt.%Mn (Al-10.75wt.%Mg-2.86wt.%Si-0.59wt.%Mn) alloy with varied Zn content under as-cast condition.

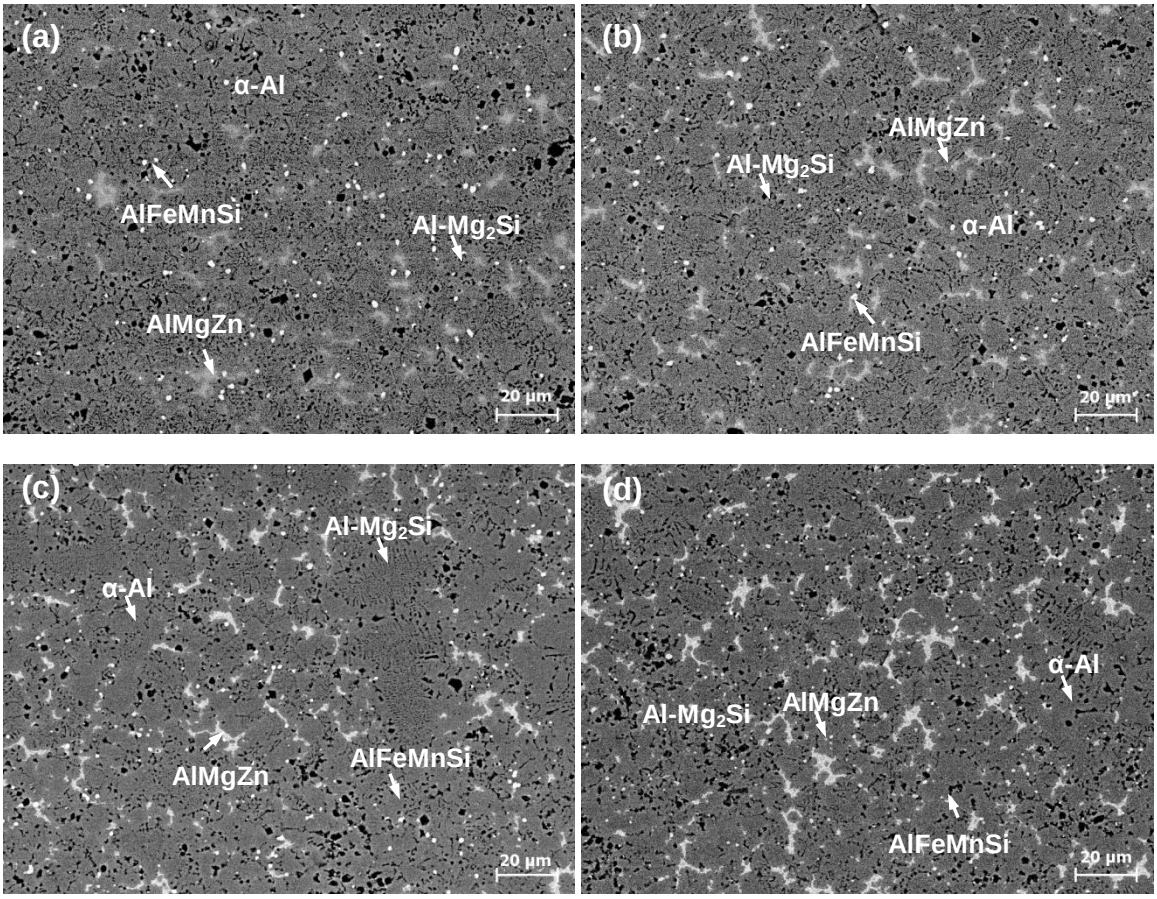

Figure 11 Backscattered SEM images showing the microstructure of the Al-7.8wt.%Mg_2Si-5.8 wt.%Mg-0.59 wt.% Mn (Al-10.75wt.%Mg-2.86wt.%Si-0.59wt.%Mn) alloy with different amount of Zn (a) 0.97wt.% Zn, (b) 1.87wt.% Zn, (c) 2.56wt.% Zn, and (d) 3.51wt.% Zn.

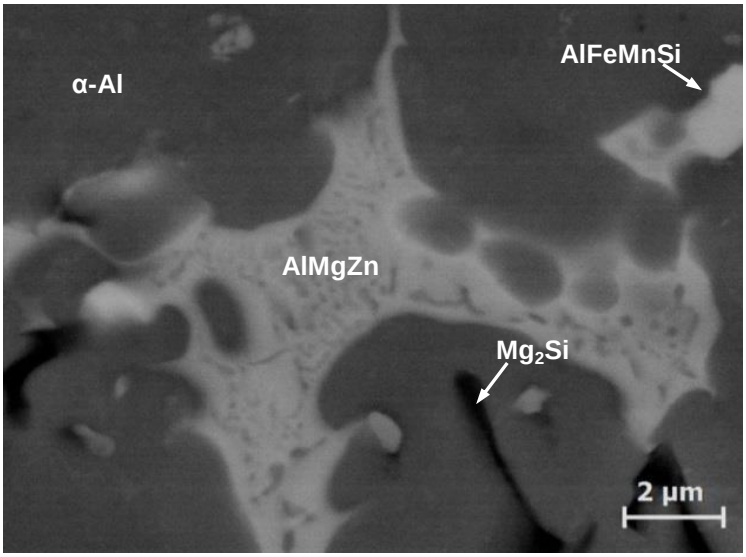

Figure 12 Backscattered SEM image showing the morphology of the AlMgZn intermetallics in the Al-7.8wt.%Mg_2Si-5.8 wt.%Mg-0.59 wt.%Mn-3.51wt.%Zn (Al-10.75wt.%Mg-2.86wt.%Si-0.59wt.%Mn-3.51wt.%Zn) alloy under as-cast condition.

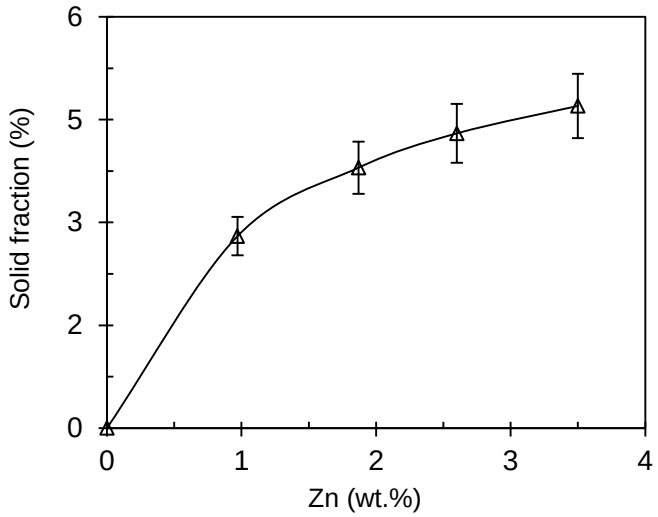

Figure 13 Solid fraction of the Zn-rich intermetallics in the Al-7.8wt.%Mg_2Si-5.8 wt.%Mg-0.59 wt.%Mn -xZn (Al-10.75wt.%Mg-2.86wt.%Si-0.59wt.%Mn-xZn) alloys.

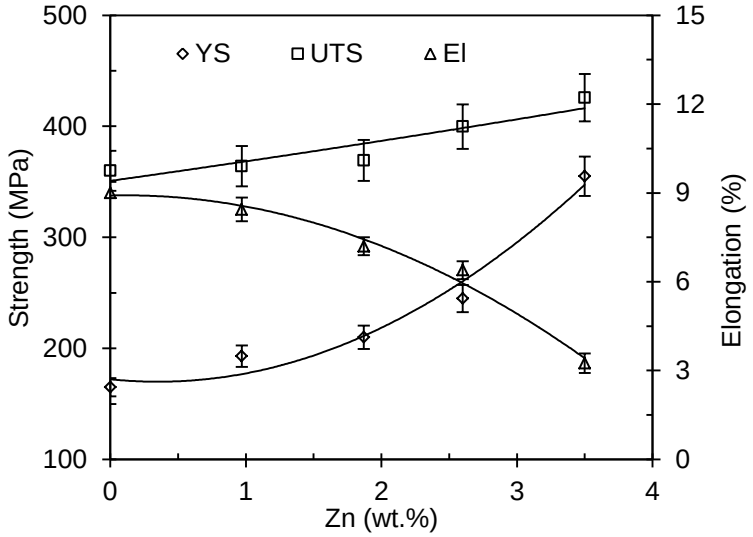

Figure 14 Mechanical properties of the Al-7.8wt.%Mg_2Si-5.8 wt.%Mg-0.59 wt.%Mn -3.51wt.%Zn (Al-10.75wt.%Mg-2.86wt.%Si-0.59wt.%Mn-3.51wt.%Zn) alloy under a condition of solution treated at 490^{o}C for 15 minutes and subsequent aged at 180^{o}C for 90 minutes.

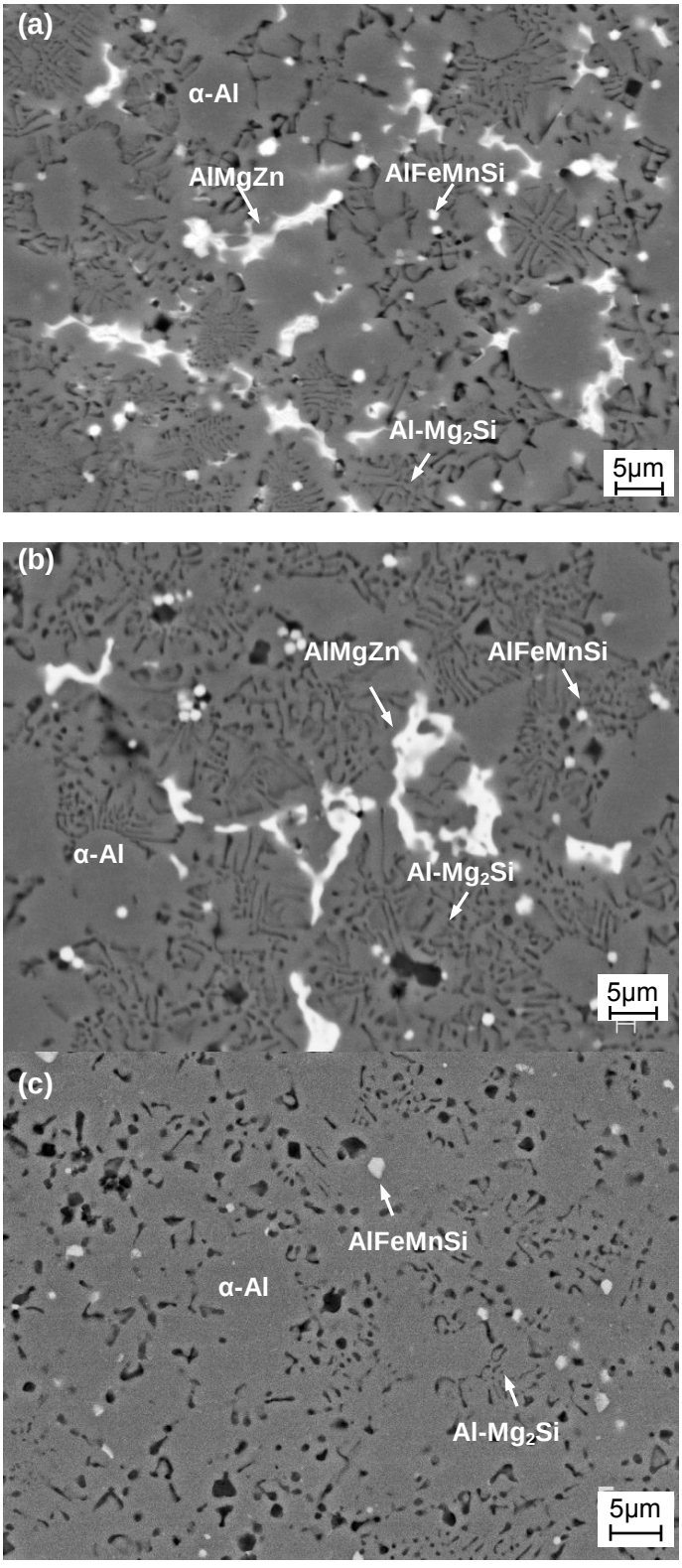

Figure 15 Backscattered SEM images showing the variation of Zn-rich intermetallic phase in the Al-7.8wt.%Mg_2Si-5.8 wt.%Mg-0.59 wt.%Mn -3.51wt.%Zn (Al-10.75wt.%Mg-2.86wt.%Si-0.59wt.%Mn-3.51 wt.%Zn) alloy (a) under as-cast condition (no solution treatment), (b) solution treated at 490°C for 10 minutes, and (c) solution heat treated at 490 °C for 15 minutes.

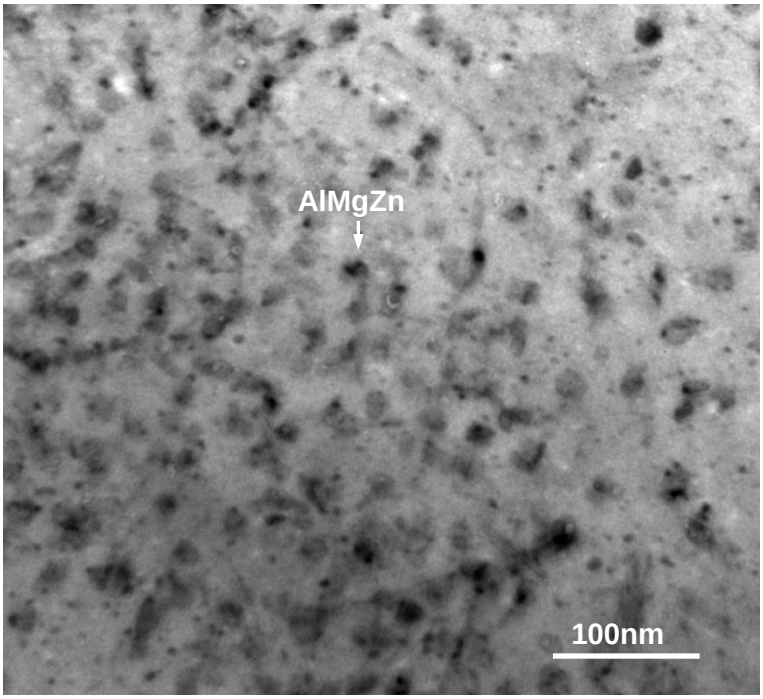

Figure 16 TEM micrographs showing the precipitates of AlMgZn phase in the α-Al phase of the Al-7.8wt.%Mg_2Si-5.8 wt.%Mg-0.59 wt.%Mn -3.51wt.%Zn (Al-10.75wt.%Mg-2.86wt.%Si-0.59wt.%Mn-3.51wt.%Zn) alloy under a condition of solution treated at 490^{o}C for 30 minutes and subsequent ageing at 180^{o}C for 60 minutes.

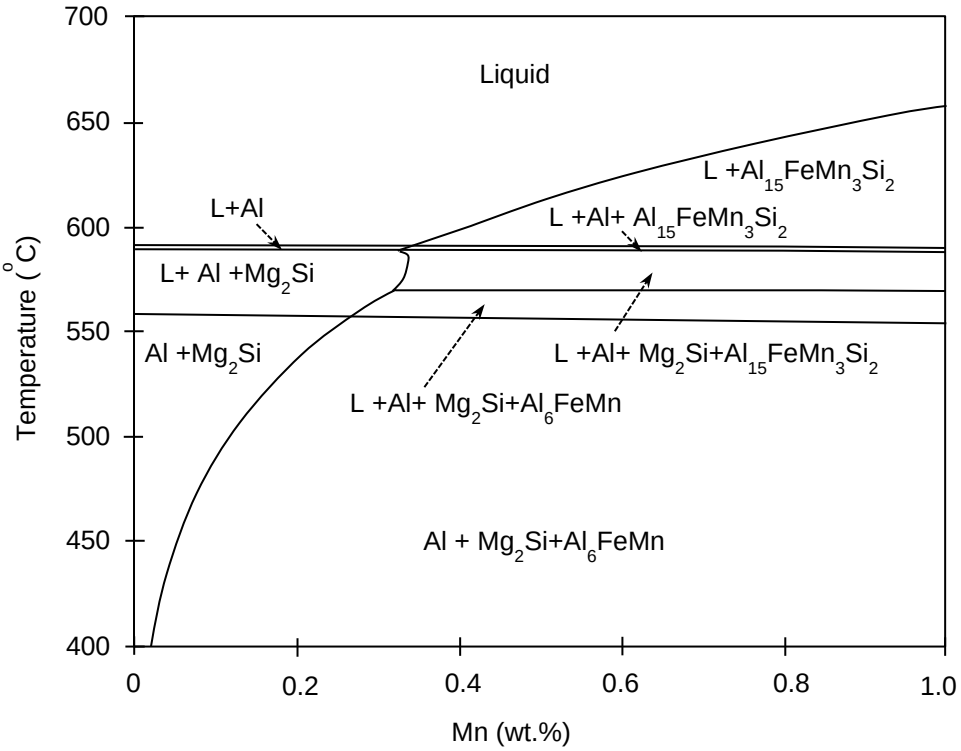

Figure 17 The equilibrium phase diagram of Al-Mg_2Si-Mg-Mn alloys on the cross section of the Al-8wt.%Mg_2Si-6 wt.%Mg (Al-11.07wt.%Mg-2.93wt.%Si) calculated by Pandat software.

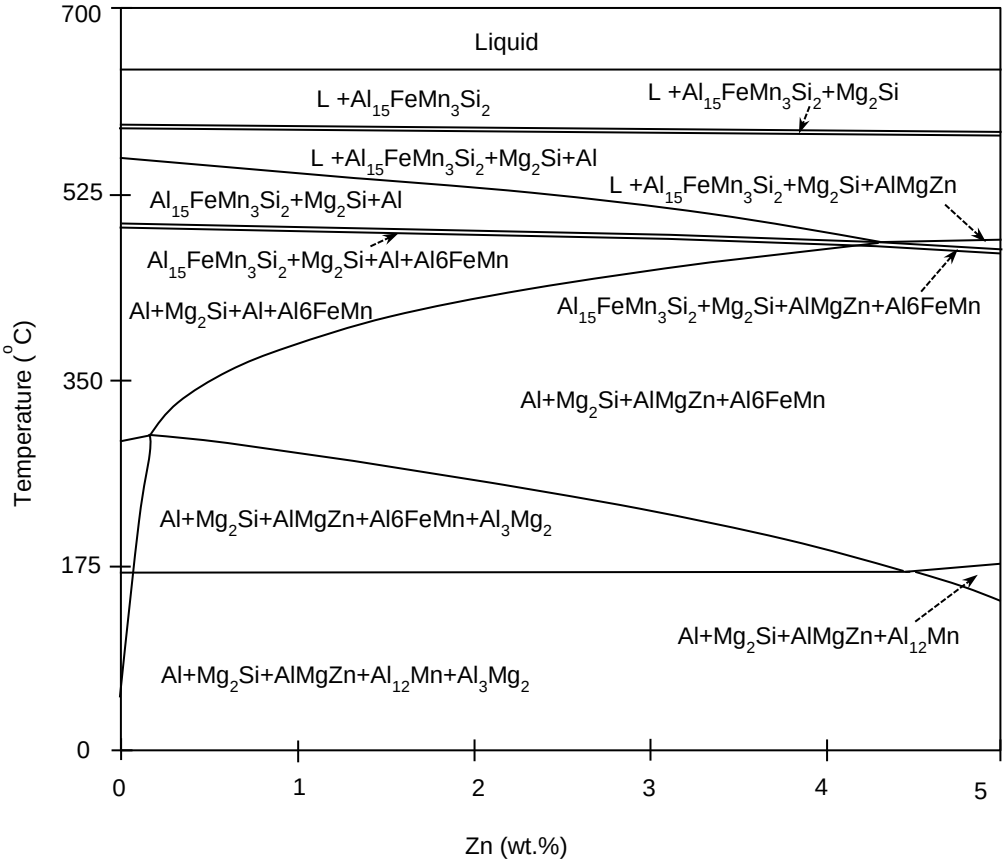

Figure 18 The equilibrium phase diagram of Al-Mg_2Si-Mg-Zn-Mn alloys on the cross section of the Al-8 wt.%Mg_2Si-6 wt.%Mg-0.6wt.%Mn (Al-11.07wt.%Mg-2.93wt.%Si-0.6wt.%Mn) calculated by Pandat software.

Reference

[1] B. Upton, Pressure Die Casting, Part 1: Metals, Machines and Furnaces, Wheaton & Co. Ltd. Exeter, UK, 1982.
[2] A, Street, The Die Casting Book, Portcullis Press Ltd, UK, 1977.
[3] S. Ji, Z. Zhen, Z. Fan, Mater. Sci. Tech. 21 (2005), 1019-1024.
[4] S. Ji, Y. Wang, D. Watson, Z. Fan, Metall. Mater. Trans. A 44 (2013), 3185-3197.
[5] M. Thirugnanam, Modern high pressure die-casting processes for aluminium castings, Transactions of 61st Indian Foundry Congress 2013, p1-7.
[6] H. I. Laukli, High pressure die casting of aluminium and magnesium alloys. Ph. D. Thesis, Norwegian University of Science and Technology, 2004.
[7] S. Ji, D. Watson, Z. Fan, M. White, Mater. Sci. Eng. A 556 (2012) 824-833.
[8] A. Badal, Y. Longa, P. Hairy, Die Casting Engineer 7 (2001) 54-60.
[9] J. R. Davis, ASM Speciality Handbook: Aluminium and Aluminium alloys, ASM International Materials Park, OH, USA, 1993.
[10] V. S. Zolotorevsky, N. A. Belov, M. V. Glazoff, Casting Aluminium Alloys, Elsevier, Oxford, ISBN: 9780080453705, UK, 2007.
[11] R. N. Lumley, I. J. Polmear, P. R. Curtis, Metal. Mater. Trans. A 40A (2009) 1716-1726.
[12] Annual Book of ASTM standards, vol. 02.02, Warrendale PA, USA, 1993.
[13] D. M. Stefanscu, J. R. Davis, J.D. Destefani (eds.), ASM metals handbook, 9th ed., vol. 15, Casting, Metals Park, OH, ASM International, 1988.
[14] G. Frommeyer, S. Beer, K. Von Oldenburg, Zeitschrift für Metallkunde 85(1994) 372-377.
[15] J. Zhang, Z. Fan, Y.Q. Wang, B.L. Zhou, Scripta Materialia, 42(2000) 1101-1106.
[16] G. E. Totten, D. S. MacKenzie (Eds.), Handbook of Aluminium: Vol. 1: Physical Metallurgy and Processes, CRC Press, Boca Raton, FL, ISBN: 978-0-203-91259-1, 2003.
[17] S.G. Shabestari, J.E. Gruzleski, Metall. Mater. Trans. 26A (1995) 999–1006.
[18] F. Yan, Development of High Strength Al-Mg_2Si-Mg Based Alloy for High Pressure Die casting Process, Ph. D. Thesis. Brunel University London, 2013.
[19] S. Ji, W. Yang, F. Gao, D. Watson, Z. Fan, Mater. Sci. Eng. A 564 (2013) 130-139.
[20] P. Villars, L.D. Calvert (eds.), Pearson's Handbook of Crystallographic Data for Intermetallic Phases, 2nd ed., Materials Park, OH, ASM International, 1991.
[21] S. Murali, K.S. Raman, K.S.S. Murthy, Mater. Sci. Eng. A, 190A (1995) 165-172.
[22] A.M. Zakharov, I.T. Guldin, A. A. Aenold, A. Yu, Matsenko. Izv. Akad. Nauk SSSR Metall. 4 (1989) 214-223.
[23] G. Davignon, A. Serneels, B. Verlinden, L. Delaey, Metall. Mater. Trans. A 27A (1996) 3357-3361.
[24] X. Fang, G. Shao, Y.Q. Liu, Z. Fan, Mater. Sci. Eng. A, 445-446 (2007) 65-72.
[25] Z. Skoko, S. Popović, G. Štefanić, Croatica Chemica Acta, 82 (2009) 405- 420.